

2 Direct Learning of Sparse Changes in 3 Markov Networks by Density Ratio Estimation*

4 Song Liu

song@sg.cs.titech.ac.jp

Tokyo Institute of Technology,

2-12-1 O-okayama, Meguro, Tokyo 152-8552, Japan.

<http://sugiyama-www.cs.titech.ac.jp/~song/>

John A. Quinn

jquinn@cit.ac.ug

Makerere University, P.O. Box 7062, Kampala, Uganda.

Michael U. Gutmann

michael.gutmann@helsinki.fi

University of Helsinki, Finland, P.O. Box 68, FI-00014, Finland.

Taiji Suzuki

suzuki.t.ct@m.titech.ac.jp

Tokyo Institute of Technology,

2-12-1 O-okayama, Meguro, Tokyo 152-8552, Japan.

Masashi Sugiyama

sugi@cs.titech.ac.jp

Tokyo Institute of Technology,

2-12-1 O-okayama, Meguro, Tokyo 152-8552, Japan.

<http://sugiyama-www.cs.titech.ac.jp/>

5 Abstract

6 We propose a new method for detecting changes in Markov network structure be-
7 tween two sets of samples. Instead of naively fitting two Markov network models
8 separately to the two data sets and figuring out their difference, we *directly* learn the
9 network structure change by estimating the ratio of Markov network models. This
10 density-ratio formulation naturally allows us to introduce sparsity in the network
11 structure change, which highly contributes to enhancing interpretability. Further-
12 more, computation of the normalization term, which is a critical bottleneck of the
13 naive approach, can be remarkably mitigated. We also give the dual formulation
14 of the optimization problem, which further reduces the computation cost for large-
15 scale Markov networks. Through experiments, we demonstrate the usefulness of our
16 method.

*An earlier version of this work was presented at the European Conference on Machine Learning and Principles and Practice of Knowledge Discovery in Databases (ECML/PKDD2013) on Sep. 23-27, 2013.

1 Introduction

Changes in interactions between random variables are interesting in many real-world phenomena. For example, genes may interact with each other in different ways when external stimuli change, co-occurrence between words may appear/disappear when the domains of text corpora shift, and correlation among pixels may change when a surveillance camera captures anomalous activities. Discovering such changes in interactions is a task of great interest in machine learning and data mining, because it provides useful insights into underlying mechanisms in many real-world applications.

In this paper, we consider the problem of detecting changes in conditional independence among random variables between two sets of data. Such conditional independence structure can be expressed via an undirected graphical model called a *Markov network* (MN) (Bishop, 2006; Wainwright and Jordan, 2008; Koller and Friedman, 2009), where nodes and edges represent variables and their conditional dependencies, respectively. As a simple and widely applicable case, the pairwise MN model has been thoroughly studied recently (Ravikumar et al., 2010; Lee et al., 2007). Following this line, we also focus on the pairwise MN model as a representative example.

A naive approach to change detection in MNs is the two-step procedure of first estimating two MNs separately from two sets of data by *maximum likelihood estimation* (MLE), and then comparing the structure of the learned MNs. However, MLE is often computationally intractable due to the normalization factor included in the density model. Therefore, Gaussianity is often assumed in practice for computing the normalization factor analytically (Hastie et al., 2001), though this Gaussian assumption is highly restrictive in practice. We may utilize *importance sampling* (Robert and Casella, 2005) to numerically compute the normalization factor, but an inappropriate choice of the instrumental distribution may lead to an estimate with high variance (Wasserman, 2010); for more discussions on sampling techniques, see Gelman (1995) and Hinton (2002). Hyvärinen (2005) and Gutmann and Hyvärinen (2012) have explored an alternative approach to avoid computing the normalization factor which are not based on MLE.

However, the two-step procedure has the conceptual weakness that structure change is not directly learned. This indirect nature causes a crucial problem: Suppose that we want to learn a sparse structure change. For learning sparse changes, we may utilize ℓ_1 -regularized MLE (Banerjee et al., 2008; Friedman et al., 2008; Lee et al., 2007), which produces sparse MNs and thus the change between MNs also becomes sparse. However, this approach does not work if each MN is dense but only change is sparse.

To mitigate this indirect nature, the *fused-lasso* (Tibshirani et al., 2005) is useful, where two MNs are simultaneously learned with a sparsity-inducing penalty on the *difference* between two MN parameters (Zhang and Wang, 2010; Danaher et al., 2013). Although this fused-lasso approach allows us to learn sparse structure change naturally, the restrictive Gaussian assumption is still necessary to obtain the solution in a computationally tractable way.

The *nonparanormal* assumption (Liu et al., 2009, 2012) is a useful generalization of the Gaussian assumption. A nonparanormal distribution is a *semi-parametric Gaussian*

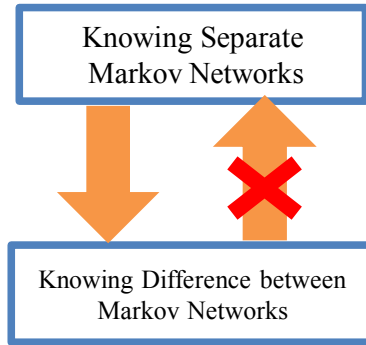


Figure 1: The rationale of direct structural change learning: finding the difference between two MNs is a more specific task than finding the entire structures of those two networks, and hence should be possible to learn with less data.

copula where each Gaussian variable is transformed by a monotone non-linear function. Nonparanormal distributions are much more flexible than Gaussian distributions thanks to the feature-wise non-linear transformation, while the normalization factors can still be computed analytically. Thus, the fused-lasso method combined with nonparanormal models would be one of the state-of-the-art approaches to change detection in MNs. However, the fused-lasso method is still based on separate modeling of two MNs, and its computation for more general non-Gaussian distributions is challenging.

In this paper, we propose a more direct approach to structural change learning in MNs based on *density ratio estimation* (DRE) (Sugiyama et al., 2012a). Our method does not separately model two MNs, but directly models the *change* in two MNs. This idea follows Vapnik’s principle (Vapnik, 1998):

If you possess a restricted amount of information for solving some problem, try to solve the problem directly and never solve a more general problem as an intermediate step. It is possible that the available information is sufficient for a direct solution but is insufficient for solving a more general intermediate problem.

This principle was used in the development of *support vector machines* (SVMs): rather than modeling two classes of samples, SVM directly learns a decision boundary that is sufficient for performing pattern recognition. In the current context, estimating two MNs is more general than detecting changes in MNs (Figure 1). By directly detecting changes in MNs, we can also halve the number of parameters, from two MNs to one MN-difference.

Another important advantage of our DRE-based method is that the normalization factor can be approximated efficiently, because the normalization term in a density ratio function takes the form of the expectation over a data distribution and thus it can be simply approximated by the sample average without additional sampling. Through experiments on gene expression and Twitter data analysis, we demonstrate the usefulness of our proposed approach.

The remainder of this paper is structured as follows. In Section 2, we formulate the problem of detecting structural changes and review currently available approaches. We then propose our DRE-based structural change detection method in Section 3. Results of illustrative and real-world experiments are reported in Section 4 and Section 5, respectively. Finally, we conclude our work and show the future direction in Section 6.

2 Problem Formulation and Related Methods

In this section, we formulate the problem of change detection in Markov network structure and review existing approaches.

2.1 Problem Formulation

Consider two sets of independent samples drawn separately from two probability distributions P and Q on \mathbb{R}^d :

$$\{\mathbf{x}_i^P\}_{i=1}^{n_P} \stackrel{\text{i.i.d.}}{\sim} P \text{ and } \{\mathbf{x}_i^Q\}_{i=1}^{n_Q} \stackrel{\text{i.i.d.}}{\sim} Q.$$

We assume that P and Q belong to the family of *Markov networks* (MNs) consisting of univariate and bivariate factors¹, i.e., their respective probability densities p and q are expressed as

$$p(\mathbf{x}; \boldsymbol{\theta}) = \frac{1}{Z(\boldsymbol{\theta})} \exp \left(\sum_{u,v=1, u \geq v}^d \boldsymbol{\theta}_{u,v}^\top \mathbf{f}(x^{(u)}, x^{(v)}) \right), \quad (1)$$

where $\mathbf{x} = (x^{(1)}, \dots, x^{(d)})^\top$ is the d -dimensional random variable, \top denotes the transpose, $\boldsymbol{\theta}_{u,v}$ is the parameter vector for the elements $x^{(u)}$ and $x^{(v)}$, and

$$\boldsymbol{\theta} = (\boldsymbol{\theta}_{1,1}^\top, \dots, \boldsymbol{\theta}_{d,1}^\top, \boldsymbol{\theta}_{2,2}^\top, \dots, \boldsymbol{\theta}_{d,2}^\top, \dots, \boldsymbol{\theta}_{d,d}^\top)^\top$$

is the entire parameter vector. $\mathbf{f}(x^{(u)}, x^{(v)})$ is a bivariate vector-valued basis function. $Z(\boldsymbol{\theta})$ is the normalization factor defined as

$$Z(\boldsymbol{\theta}) = \int \exp \left(\sum_{u,v=1, u \geq v}^d \boldsymbol{\theta}_{u,v}^\top \mathbf{f}(x^{(u)}, x^{(v)}) \right) d\mathbf{x}.$$

$q(\mathbf{x}; \boldsymbol{\theta})$ is defined in the same way.

Given two densities which can be parameterized using $p(\mathbf{x}; \boldsymbol{\theta}^P)$ and $q(\mathbf{x}; \boldsymbol{\theta}^Q)$, our goal is to discover *the changes in parameters* from P to Q , i.e., $\boldsymbol{\theta}^P - \boldsymbol{\theta}^Q$.

¹Note that the proposed algorithm itself can be applied to *any* MNs containing more than two elements in each factor.

2.2 Sparse Maximum Likelihood Estimation and Graphical Lasso

Maximum likelihood estimation (MLE) with group ℓ_1 -regularization has been widely used for estimating the sparse structure of MNs (Schmidt and Murphy, 2010; Ravikumar et al., 2010; Lee et al., 2007):

$$\max_{\boldsymbol{\theta}} \left[\frac{1}{n_P} \sum_{i=1}^{n_P} \log p(\mathbf{x}_i^P; \boldsymbol{\theta}) - \lambda \sum_{u,v=1, u \geq v}^d \|\boldsymbol{\theta}_{u,v}\| \right], \quad (2)$$

where $\|\cdot\|$ denotes the ℓ_2 -norm. As λ increases, $\|\boldsymbol{\theta}_{u,v}\|$ may drop to 0. Thus, this method favors an MN that encodes more conditional independencies among variables.

Computation of the normalization term $Z(\boldsymbol{\theta})$ in Eq.(1) is often computationally intractable when the dimensionality of \mathbf{x} is high. To avoid this computational problem, the Gaussian assumption is often imposed (Friedman et al., 2008; Meinshausen and Bühlmann, 2006). More specifically, the following zero-mean Gaussian model is used:

$$p(\mathbf{x}; \boldsymbol{\Theta}) = \frac{\det(\boldsymbol{\Theta})^{1/2}}{(2\pi)^{d/2}} \exp \left(-\frac{1}{2} \mathbf{x}^\top \boldsymbol{\Theta} \mathbf{x} \right),$$

where $\boldsymbol{\Theta}$ is the inverse covariance matrix (a.k.a. the precision matrix) and $\det(\cdot)$ denotes the determinant. Then $\boldsymbol{\Theta}$ is learned as

$$\max_{\boldsymbol{\Theta}} [\log \det(\boldsymbol{\Theta}) - \text{tr}(\boldsymbol{\Theta} \mathbf{S}^P) - \lambda \|\boldsymbol{\Theta}\|_1],$$

where \mathbf{S}^P is the sample covariance matrix of $\{\mathbf{x}_i^P\}_{i=1}^n$. $\|\boldsymbol{\Theta}\|_1$ is the ℓ_1 -norm of $\boldsymbol{\Theta}$, i.e., the absolute sum of all elements. This formulation has been studied intensively in Banerjee et al. (2008), and a computationally efficient algorithm called the *graphical lasso* (Glasso) has been proposed (Friedman et al., 2008).

Sparse changes in conditional independence structure between P and Q can be detected by comparing two MNs estimated separately using sparse MLE. However, this approach implicitly assumes that two MNs are sparse, which is not necessarily true even if the change is sparse.

2.3 Fused-Lasso (Flasso) Method

To more naturally handle sparse changes in conditional independence structure between P and Q , a method based on *fused-lasso* (Tibshirani et al., 2005) has been developed (Zhang and Wang, 2010). This method directly sparsifies the *difference* between parameters.

The original method conducts *feature-wise neighborhood regression* (Meinshausen and Bühlmann, 2006) jointly for P and Q , which can be conceptually understood as maximizing the local conditional Gaussian likelihood jointly on each feature (Ravikumar et al., 2010). A slightly more general form of the learning criterion may be summarized as

$$\max_{\boldsymbol{\theta}_s^P, \boldsymbol{\theta}_s^Q} [\ell_s^P(\boldsymbol{\theta}_s^P) + \ell_s^Q(\boldsymbol{\theta}_s^Q) - \lambda_1 (\|\boldsymbol{\theta}_s^P\|_1 + \|\boldsymbol{\theta}_s^Q\|_1) - \lambda_2 \|\boldsymbol{\theta}_s^P - \boldsymbol{\theta}_s^Q\|_1],$$

where $\ell_s^P(\boldsymbol{\theta})$ is the log conditional likelihood for the s -th element $x^{(s)} \in \mathbb{R}$ given the rest $\mathbf{x}^{(-s)} \in \mathbb{R}^{d-1}$:

$$\ell_s^P(\boldsymbol{\theta}) = \frac{1}{n_P} \sum_{i=1}^{n_P} \log p(x_i^{(s)P} | \mathbf{x}_i^{(-s)P}; \boldsymbol{\theta}).$$

$\ell_s^Q(\boldsymbol{\theta})$ is defined in the same way as $\ell_s^P(\boldsymbol{\theta})$.

Since the Flasso-based method directly sparsifies the change in MN structure, it can work well even when each MN is not sparse. However, using other models than Gaussian is difficult because of the normalization issue described in Section 2.2.

2.4 Nonparanormal Extensions

In the above methods, Gaussianity is required in practice to compute the normalization factor efficiently, which is a highly restrictive assumption. To overcome this restriction, it has become popular to perform structure learning under the *nonparanormal* settings (Liu et al., 2009, 2012), where the Gaussian distribution is replaced by a *semi-parametric Gaussian copula*.

A random vector $\mathbf{x} = (x^{(1)}, \dots, x^{(d)})^\top$ is said to follow a *nonparanormal* distribution, if there exists a set of monotone and differentiable functions, $\{h_i(x)\}_{i=1}^d$, such that $\mathbf{h}(\mathbf{x}) = (h_1(x^{(1)}), \dots, h_d(x^{(d)}))^\top$ follows the Gaussian distribution. Nonparanormal distributions are much more flexible than Gaussian distributions thanks to the non-linear transformation $\{h_i(x)\}_{i=1}^d$, while the normalization factors can still be computed in an analytical way.

However, the nonparanormal transformation is restricted to be element-wise, which is still restrictive to express complex distributions.

2.5 Maximum Likelihood Estimation for Non-Gaussian Models by Importance-Sampling

A numerical way to obtain the MLE solution under general non-Gaussian distributions is *importance sampling*.

Suppose that we try to maximize the log-likelihood²:

$$\begin{aligned} \ell_{\text{MLE}}(\boldsymbol{\theta}) &= \frac{1}{n_P} \sum_{i=1}^{n_P} \log p(\mathbf{x}_i^P; \boldsymbol{\theta}) \\ &= \frac{1}{n_P} \sum_{i=1}^{n_P} \sum_{u \geq v} \boldsymbol{\theta}_{u,v}^\top \mathbf{f}(x_i^{(u)P}, x_i^{(v)P}) - \log \int \exp \left(\sum_{u \geq v} \boldsymbol{\theta}_{u,v}^\top \mathbf{f}(x^{(u)}, x^{(v)}) \right) d\mathbf{x}. \end{aligned} \quad (3)$$

The key idea of importance sampling is to compute the integral by the expectation over an easy-to-sample *instrumental density* $p'(\mathbf{x})$ (e.g., Gaussian) weighted according to

²From here on, we simplify $\sum_{u,v=1, u \geq v}^d$ as $\sum_{u \geq v}$.

the *importance* $1/p'(\mathbf{x})$. More specifically, using i.i.d. samples $\{\mathbf{x}'_i\}_{i=1}^{n'} \stackrel{\text{i.i.d.}}{\sim} p'(\mathbf{x})$, the last term of Eq.(3) can be approximately computed as follows:

$$\begin{aligned} \log \int \exp \left(\sum_{u \geq v} \boldsymbol{\theta}_{u,v}^\top \mathbf{f}(x^{(u)}, x^{(v)}) \right) d\mathbf{x} &= \log \int p'(\mathbf{x}) \frac{\exp \left(\sum_{u \geq v} \boldsymbol{\theta}_{u,v}^\top \mathbf{f}(x^{(u)}, x^{(v)}) \right)}{p'(\mathbf{x})} d\mathbf{x} \\ &\approx \log \frac{1}{n'} \sum_{i=1}^{n'} \frac{\exp \left(\sum_{u \geq v} \boldsymbol{\theta}_{u,v}^\top \mathbf{f}(x_i^{(u)}, x_i^{(v)}) \right)}{p'(\mathbf{x}'_i)}. \end{aligned}$$

We refer to this implementation of Glasso as IS-Glasso below.

However, importance sampling tends to produce an estimate with large variance if the instrumental distribution is not carefully chosen. Although it is often suggested to use a density whose shape is similar to the function to be integrated but with thicker tails as p' , it is not straightforward in practice to decide which p' to choose, especially when the dimensionality of \mathbf{x} is high (Wasserman, 2010).

We can also consider an importance-sampling version of the Flasso method (which we refer to as IS-Flasso)³

$$\max_{\boldsymbol{\theta}^P, \boldsymbol{\theta}^Q} \left[\ell_{\text{MLE}}^P(\boldsymbol{\theta}^P) + \ell_{\text{MLE}}^Q(\boldsymbol{\theta}^Q) - \lambda_1 (\|\boldsymbol{\theta}^P\|^2 + \|\boldsymbol{\theta}^Q\|^2) - \lambda_2 \sum_{u \geq v} \|\boldsymbol{\theta}_{u,v}^P - \boldsymbol{\theta}_{u,v}^Q\| \right],$$

where both $\ell_{\text{MLE}}^P(\boldsymbol{\theta}^P)$ and $\ell_{\text{MLE}}^Q(\boldsymbol{\theta}^Q)$ are approximated by importance sampling for non-Gaussian distributions. However, in the same way as IS-Glasso, the choice of instrumental distributions is not straightforward.

3 Direct Learning of Structural Changes via Density Ratio Estimation

The Flasso method can more naturally handle sparse changes in MNs than separate sparse MLE. However, the Flasso method is still based on separate modeling of two MNs, and its computation for general high-dimensional non-Gaussian distributions is challenging. In this section, we propose to directly learn structural changes based on *density ratio estimation* (Sugiyama et al., 2012a). Our approach does not involve separate modeling of each MN and allows us to approximate the normalization term efficiently for *any* distributions.

3.1 Density Ratio Formulation for Structural Change Detection

Our key idea is to consider the ratio of p and q :

³For implementation simplicity, we maximize the joint likelihood of p and q , instead of its feature-wise conditional likelihood. We also switch the first penalty term from ℓ_1 to ℓ_2 .

$$\frac{p(\mathbf{x}; \boldsymbol{\theta}^P)}{q(\mathbf{x}; \boldsymbol{\theta}^Q)} \propto \exp \left(\sum_{u \geq v} (\boldsymbol{\theta}_{u,v}^P - \boldsymbol{\theta}_{u,v}^Q)^\top \mathbf{f}(x^{(u)}, x^{(v)}) \right).$$

156 Here $\boldsymbol{\theta}_{u,v}^P - \boldsymbol{\theta}_{u,v}^Q$ encodes the difference between P and Q for factor $\mathbf{f}(x^{(u)}, x^{(v)})$, i.e.,
 157 $\boldsymbol{\theta}_{u,v}^P - \boldsymbol{\theta}_{u,v}^Q$ is zero if there is no change in the factor $\mathbf{f}(x^{(u)}, x^{(v)})$.

Once we consider the ratio of p and q , we actually do not have to estimate $\boldsymbol{\theta}_{u,v}^P$ and $\boldsymbol{\theta}_{u,v}^Q$; instead estimating their difference $\boldsymbol{\theta}_{u,v} = \boldsymbol{\theta}_{u,v}^P - \boldsymbol{\theta}_{u,v}^Q$ is sufficient for change detection:

$$r(\mathbf{x}; \boldsymbol{\theta}) = \frac{1}{N(\boldsymbol{\theta})} \exp \left(\sum_{u \geq v} \boldsymbol{\theta}_{u,v}^\top \mathbf{f}(x^{(u)}, x^{(v)}) \right), \quad (4)$$

where

$$N(\boldsymbol{\theta}) = \int q(\mathbf{x}) \exp \left(\sum_{u \geq v} \boldsymbol{\theta}_{u,v}^\top \mathbf{f}(x^{(u)}, x^{(v)}) \right) d\mathbf{x}.$$

The normalization term $N(\boldsymbol{\theta})$ guarantees⁴

$$\int q(\mathbf{x}) r(\mathbf{x}; \boldsymbol{\theta}) d\mathbf{x} = 1.$$

158 Thus, in this density ratio formulation, we are no longer modeling p and q separately,
 159 but we model the change from p to q *directly*. This direct nature would be more suitable

⁴If the model $q(\mathbf{x}; \boldsymbol{\theta}^Q)$ is correctly specified, i.e., there exists $\boldsymbol{\theta}^{Q*}$ such that $q(\mathbf{x}; \boldsymbol{\theta}^{Q*}) = q(\mathbf{x})$, then $N(\boldsymbol{\theta})$ can be interpreted as importance sampling of $Z(\boldsymbol{\theta}^P)$ via instrumental distribution $q(\mathbf{x})$. Indeed, since

$$Z(\boldsymbol{\theta}^P) = \int q(\mathbf{x}) \frac{\exp \left(\sum_{u \geq v} \boldsymbol{\theta}_{u,v}^P{}^\top \mathbf{f}(x^{(u)}, x^{(v)}) \right)}{q(\mathbf{x}; \boldsymbol{\theta}^{Q*})} d\mathbf{x},$$

where $q(\mathbf{x}; \boldsymbol{\theta}^{Q*}) = q(\mathbf{x})$, we have

$$N(\boldsymbol{\theta}^P - \boldsymbol{\theta}^{Q*}) = \frac{Z(\boldsymbol{\theta}^P)}{Z(\boldsymbol{\theta}^{Q*})} = \int q(\mathbf{x}) \exp \left(\sum_{u \geq v} (\boldsymbol{\theta}_{u,v}^P - \boldsymbol{\theta}_{u,v}^{Q*})^\top \mathbf{f}(x^{(u)}, x^{(v)}) \right) d\mathbf{x}.$$

This is exactly the normalization term $N(\boldsymbol{\theta})$ of the ratio $p(\mathbf{x}; \boldsymbol{\theta}^P)/q(\mathbf{x}; \boldsymbol{\theta}^{Q*})$. However, we note that the density ratio estimation method we use in this paper is consistent to the optimal solution in the model even without the correct model assumption (Kanamori et al., 2010). An alternative normalization term,

$$N'(\boldsymbol{\theta}, \boldsymbol{\theta}^Q) = \int q(\mathbf{x}; \boldsymbol{\theta}^Q) r(\mathbf{x}; \boldsymbol{\theta}) d\mathbf{x},$$

may also be considered, as in the case of MLE. However, this alternative form requires an extra parameter $\boldsymbol{\theta}^Q$ which is not our main interest.

for change detection purposes according to Vapnik’s principle that encourages avoidance of solving more general problems as an intermediate step (Vapnik, 1998). This direct formulation also allows us to halve the number of parameters from both $\boldsymbol{\theta}^P$ and $\boldsymbol{\theta}^Q$ to only $\boldsymbol{\theta}$.

Furthermore, the normalization factor $N(\boldsymbol{\theta})$ in the density ratio formulation can be easily approximated by the sample average over $\{\mathbf{x}_i^Q\}_{i=1}^{n_Q} \stackrel{\text{i.i.d.}}{\sim} q(\mathbf{x})$, because $N(\boldsymbol{\theta})$ is the expectation over $q(\mathbf{x})$:

$$N(\boldsymbol{\theta}) \approx \frac{1}{n_Q} \sum_{i=1}^{n_Q} \exp \left(\sum_{u \geq v} \boldsymbol{\theta}_{u,v}^\top \mathbf{f}(x_i^{(u)Q}, x_i^{(v)Q}) \right).$$

3.2 Direct Density-Ratio Estimation

Density ratio estimation has been recently introduced to the machine learning community and is proven to be useful in a wide range of applications (Sugiyama et al., 2012a). Here, we concentrate on the density ratio estimator called the *Kullback-Leibler importance estimation procedure* (KLIEP) for log-linear models (Sugiyama et al., 2008; Tsuboi et al., 2009).

For a density ratio model $r(\mathbf{x}; \boldsymbol{\theta})$, the KLIEP method minimizes the Kullback-Leibler divergence from $p(\mathbf{x})$ to $\hat{p}(\mathbf{x}) = q(\mathbf{x})r(\mathbf{x}; \boldsymbol{\theta})$:

$$\begin{aligned} \text{KL}[p \parallel \hat{p}] &= \int p(\mathbf{x}) \log \frac{p(\mathbf{x})}{q(\mathbf{x})r(\mathbf{x}; \boldsymbol{\theta})} d\mathbf{x} \\ &= \text{Const.} - \int p(\mathbf{x}) \log r(\mathbf{x}; \boldsymbol{\theta}) d\mathbf{x}. \end{aligned} \quad (5)$$

Note that our density-ratio model (4) automatically satisfies the non-negativity and normalization constraints:

$$r(\mathbf{x}; \boldsymbol{\theta}) \geq 0 \quad \text{and} \quad \int q(\mathbf{x})r(\mathbf{x}; \boldsymbol{\theta}) d\mathbf{x} = 1.$$

In practice, we maximize the empirical approximation of the second term in Eq.(5):

$$\begin{aligned} \ell_{\text{KLIEP}}(\boldsymbol{\theta}) &= \frac{1}{n_P} \sum_{i=1}^{n_P} \log r(\mathbf{x}_i^P; \boldsymbol{\theta}) \\ &= \frac{1}{n_P} \sum_{i=1}^{n_P} \sum_{u \geq v} \boldsymbol{\theta}_{u,v}^\top \mathbf{f}(x_i^{(u)P}, x_i^{(v)P}) \\ &\quad - \log \left(\frac{1}{n_Q} \sum_{i=1}^{n_Q} \exp \left(\sum_{u \geq v} \boldsymbol{\theta}_{u,v}^\top \mathbf{f}(x_i^{(u)Q}, x_i^{(v)Q}) \right) \right). \end{aligned}$$

Because $\ell_{\text{KLIEP}}(\boldsymbol{\theta})$ is concave with respect to $\boldsymbol{\theta}$, its global maximizer can be numerically found by standard optimization techniques such as gradient ascent or quasi-Newton

methods. The gradient of ℓ_{KLIEP} with respect to $\boldsymbol{\theta}_{u,v}$ is given by

$$\begin{aligned} \nabla_{\boldsymbol{\theta}_{u,v}} \ell_{\text{KLIEP}}(\boldsymbol{\theta}) = & \frac{1}{n_P} \sum_{i=1}^{n_P} \mathbf{f}(\mathbf{x}_i^{(u)P}, \mathbf{x}_i^{(v)P}) \\ & - \frac{\frac{1}{n_Q} \sum_{i=1}^{n_Q} \exp\left(\sum_{u' \geq v'} \boldsymbol{\theta}_{u',v'}^\top \mathbf{f}(\mathbf{x}_i^{(u')Q}, \mathbf{x}_i^{(v')Q})\right) \mathbf{f}(\mathbf{x}_i^{(u)Q}, \mathbf{x}_i^{(v)Q})}{\frac{1}{n_Q} \sum_{j=1}^{n_Q} \exp\left(\sum_{u'' \geq v''} \boldsymbol{\theta}_{u'',v''}^\top \mathbf{f}(\mathbf{x}_j^{(u'')Q}, \mathbf{x}_j^{(v'')Q})\right)}, \end{aligned}$$

170 which can be computed in a straightforward manner for *any* feature vector $\mathbf{f}(x^{(u)}, x^{(v)})$.

171 3.3 Sparsity-Inducing Norm

172 To find a sparse change between P and Q , we propose to regularize the KLIEP solution
173 with a sparsity-inducing norm $\sum_{u \geq v} \|\boldsymbol{\theta}_{u,v}\|$. Note that the MLE approach sparsifies both
174 $\boldsymbol{\theta}^P$ and $\boldsymbol{\theta}^Q$ so that the difference $\boldsymbol{\theta}^P - \boldsymbol{\theta}^Q$ is also sparsified, while we directly sparsify the
175 difference $\boldsymbol{\theta}^P - \boldsymbol{\theta}^Q$; thus our method can still work well even if $\boldsymbol{\theta}^P$ and $\boldsymbol{\theta}^Q$ are dense.

In practice, we may use the following *elastic-net* penalty (Zou and Hastie, 2005) to better control overfitting to noisy data:

$$\max_{\boldsymbol{\theta}} \left[\ell_{\text{KLIEP}}(\boldsymbol{\theta}) - \lambda_1 \|\boldsymbol{\theta}\|^2 - \lambda_2 \sum_{u \geq v} \|\boldsymbol{\theta}_{u,v}\| \right], \quad (6)$$

176 where $\|\boldsymbol{\theta}\|^2$ penalizes the magnitude of the entire parameter vector.

177 3.4 Dual Formulation for High-Dimensional Data

178 The solution of the optimization problem (6) can be easily obtained by standard sparse
179 optimization methods. However, in the case where the input dimensionality d is high
180 (which is often the case in our setup), the dimensionality of parameter vector $\boldsymbol{\theta}$ is large,
181 and thus obtaining the solution can be computationally expensive. Here, we derive a
182 dual optimization problem (Boyd and Vandenberghe, 2004), which can be solved more
183 efficiently for high-dimensional $\boldsymbol{\theta}$ (Figure 2).

As detailed in Appendix, the dual optimization problem is given as

$$\begin{aligned} \min_{\boldsymbol{\alpha}=(\alpha_1, \dots, \alpha_{n_Q})^\top} & \sum_{i=1}^{n_Q} \alpha_i \log \alpha_i + \frac{1}{\lambda_1} \sum_{u \geq v} \max(0, \|\boldsymbol{\xi}_{u,v}\| - \lambda_2)^2 \\ \text{subject to } & \alpha_1, \dots, \alpha_{n_Q} \geq 0 \text{ and } \sum_{i=1}^{n_Q} \alpha_i = 1, \end{aligned} \quad (7)$$

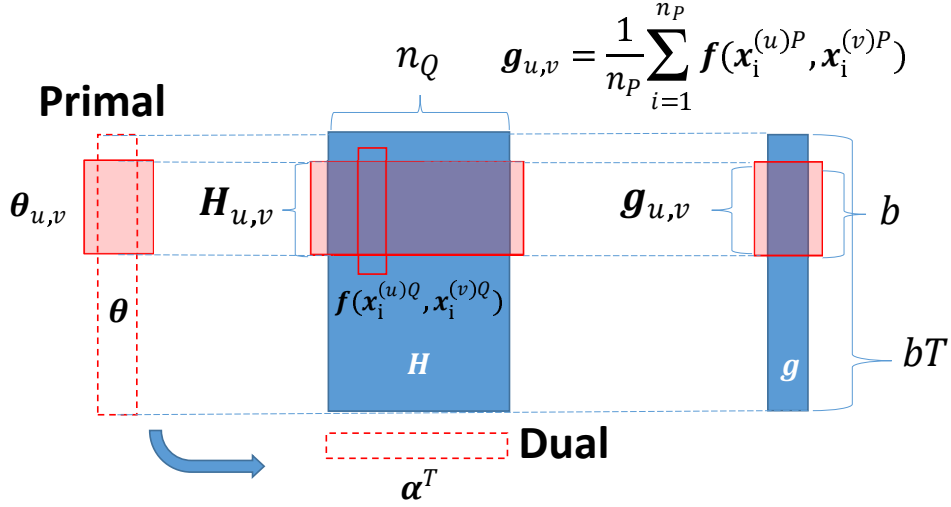


Figure 2: Schematics of primal and dual optimization. b denotes the number of basis functions and T denotes the number of factors. Because we are considering pairwise factors, $T = \mathcal{O}(d^2)$ for input dimensionality d .

where

$$\begin{aligned}\xi_{u,v} &= g_{u,v} - H_{u,v}\alpha, \\ H_{u,v} &= [f(x_1^{(u)Q}, x_1^{(v)Q}), \dots, f(x_{n_Q}^{(u)Q}, x_{n_Q}^{(v)Q})], \\ g_{u,v} &= \frac{1}{n_P} \sum_{i=1}^{n_P} f(x_i^{(u)P}, x_i^{(v)P}).\end{aligned}$$

The primal solution can be obtained from the dual solution as

$$\theta_{u,v} = \begin{cases} \frac{1}{\lambda_1} \left(1 - \frac{\lambda_2}{\|\xi_{u,v}\|}\right) \xi_{u,v} & \text{if } \|\xi_{u,v}\| > \lambda_2, \\ 0 & \text{if } \|\xi_{u,v}\| \leq \lambda_2. \end{cases} \quad (8)$$

184 Note that the dimensionality of the dual variable α is equal to n_Q , while that of
 185 θ is quadratic with respect to the input dimensionality d , because we are considering
 186 pairwise factors. Thus, if d is not small and n_Q is not very large (which is often the
 187 case in our experiments shown later), solving the dual optimization problem would be
 188 computationally more efficient. Furthermore, the dual objective (and its gradient) can be
 189 computed efficiently in parallel for each (u, v) , which is a useful property when handling
 190 large-scale MNs. Note that the dual objective is differentiable everywhere, while the
 191 primal objective is not.

4 Numerical Experiments

In this section, we compare the performance of the proposed KLIEP-based method, the Flasso method, and the Glasso method for Gaussian models, nonparanormal models, and non-Gaussian models. Results are reported on datasets with three different underlying distributions: multivariate Gaussian, nonparanormal, and non-Gaussian “diamond” distributions. We also investigate the computation time of the primal and dual formulations as a function of the input dimensionality. The MATLAB implementation of the primal and dual methods are available at

<http://sugiyama-www.cs.titech.ac.jp/~song/SCD.html>.

4.1 Gaussian Distribution

First, we investigate the performance of each method under Gaussianity.

Consider a 40-node sparse Gaussian MN, where its graphical structure is characterized by precision matrix Θ^P with diagonal elements equal to 2. The off-diagonal elements are randomly chosen⁵ and set to 0.2, so that the overall sparsity of Θ^P is 25%. We then introduce changes by randomly picking 15 edges and reducing the corresponding elements in the precision matrix by 0.1. The resulting precision matrices Θ^P and Θ^Q are used for drawing samples as

$$\{\mathbf{x}_i^P\}_{i=1}^{n_P} \stackrel{\text{i.i.d.}}{\sim} \mathcal{N}(\mathbf{0}, (\Theta^P)^{-1}) \quad \text{and} \quad \{\mathbf{x}_i^Q\}_{i=1}^{n_Q} \stackrel{\text{i.i.d.}}{\sim} \mathcal{N}(\mathbf{0}, (\Theta^Q)^{-1}),$$

where $\mathcal{N}(\boldsymbol{\mu}, \boldsymbol{\Sigma})$ denotes the multivariate normal distribution with mean $\boldsymbol{\mu}$ and covariance matrix $\boldsymbol{\Sigma}$. Datasets of size $n = n_P = n_Q = 50, 100$ are tested.

We compare the performance of the KLIEP, Flasso, and Glasso methods. Because all methods use the same Gaussian model, the difference in performance is caused only by the difference in estimation methods. We repeat the experiments 20 times with randomly generated datasets and report the results in Figure 3.

The top 6 graphs are examples of regularization paths⁶. The dashed lines represent changed edges in the ground truth, while the solid lines represent unchanged edges. The top row is for $n = 100$ while the middle row is for $n = 50$. The bottom 3 graphs are the data generating distribution and averaged precision-recall (P-R) curves with standard error over 20 runs. The P-R curves are plotted by varying the group-sparsity control parameter λ_2 with $\lambda_1 = 0$ in KLIEP and Flasso, and by varying the sparsity control parameters as $\lambda = \lambda^P = \lambda^Q$ in Glasso.

In the regularization path plots, solid vertical lines show the regularization parameter values picked based on hold-out data $\{\tilde{\mathbf{x}}_i^P\}_{i=1}^{3000} \stackrel{\text{i.i.d.}}{\sim} P$ and $\{\tilde{\mathbf{x}}_i^Q\}_{i=1}^{3000} \stackrel{\text{i.i.d.}}{\sim} Q$ as follows:

⁵We set $\Theta_{u,v} = \Theta_{v,u}$ for not breaking the symmetry of the precision matrix.

⁶Paths of univariate factors are omitted for clear visibility.

- **KLIEP:** The *hold-out log-likelihood* (HOLL) is maximized:

$$\frac{1}{\tilde{n}_P} \sum_{i=1}^{\tilde{n}_P} \log \frac{\exp \left(\sum_{u \geq v} \hat{\boldsymbol{\theta}}_{u,v}^\top \mathbf{f}(\tilde{x}_i^{(u)P}, \tilde{x}_i^{(v)P}) \right)}{\frac{1}{\tilde{n}_Q} \sum_{j=1}^{\tilde{n}_Q} \exp \left(\sum_{u' \geq v'} \hat{\boldsymbol{\theta}}_{u',v'}^\top \mathbf{f}(\tilde{x}_j^{(u')Q}, \tilde{x}_j^{(v')Q}) \right)}.$$

- **Flasso:** The sum of feature-wise conditional HOLLs for $p(\mathbf{x}^{(s)} | \mathbf{x}^{(-s)}; \boldsymbol{\theta}_s)$ and $q(\mathbf{x}^{(s)} | \mathbf{x}^{(-s)}; \boldsymbol{\theta}_s)$ over all nodes is maximized:

$$\frac{1}{\tilde{n}_P} \sum_{i=1}^{\tilde{n}_P} \sum_{s=1}^d \log p(\tilde{x}_i^{(s)P} | \tilde{\mathbf{x}}_i^{(-s)P}; \hat{\boldsymbol{\theta}}_s^P) + \frac{1}{\tilde{n}_Q} \sum_{i=1}^{\tilde{n}_Q} \sum_{s=1}^d \log q(\tilde{x}_i^{(s)Q} | \tilde{\mathbf{x}}_i^{(-s)Q}; \hat{\boldsymbol{\theta}}_s^Q).$$

- **Gllasso:** The sum of HOLLs for $p(\mathbf{x}; \boldsymbol{\theta})$ and $q(\mathbf{x}; \boldsymbol{\theta})$ is maximized:

$$\frac{1}{\tilde{n}_P} \sum_{i=1}^{\tilde{n}_P} \log p(\tilde{\mathbf{x}}_i^P; \hat{\boldsymbol{\theta}}^P) + \frac{1}{\tilde{n}_Q} \sum_{i=1}^{\tilde{n}_Q} \log q(\tilde{\mathbf{x}}_i^Q; \hat{\boldsymbol{\theta}}^Q).$$

When $n = 100$, KLIEP and Flasso clearly distinguish changed (dashed lines) and unchanged (solid lines) edges in terms of parameter magnitude. However, when the sample size is halved to $n = 50$, the separation is visually rather unclear in the case of Flasso. In contrast, the paths of changed and unchanged edges are still almost disjoint in the case of KLIEP. The Gllasso method performs rather poorly in both cases. A similar tendency can be observed also in the P-R curve plot: When the sample size is $n = 100$, KLIEP and Flasso work equally well, but KLIEP gains its lead when the sample size is reduced to $n = 50$. Gllasso does not perform well in both cases.

4.2 Nonparanormal Distribution

We post-process the Gaussian dataset used in Section 4.1 to construct nonparanormal samples. More specifically, we apply the power function,

$$h_i^{-1}(x) = \text{sign}(x)|x|^{\frac{1}{2}},$$

to each dimension of \mathbf{x}^P and \mathbf{x}^Q , so that $\mathbf{h}(\mathbf{x}^P) \sim \mathcal{N}(\mathbf{0}, (\boldsymbol{\Theta}^P)^{-1})$ and $\mathbf{h}(\mathbf{x}^Q) \sim \mathcal{N}(\mathbf{0}, (\boldsymbol{\Theta}^Q)^{-1})$.

To cope with the non-linearity in the KLIEP method, we use the power nonparanormal basis functions with power $k = 2, 3$, and 4:

$$\mathbf{f}(x_i, x_j) = (\text{sign}(x_i)|x_i|^k, \text{sign}(x_j)|x_j|^k, 1)^\top.$$

Model selection of k is performed together with the regularization parameter by HOLL maximization. For Flasso and Gllasso, we apply the nonparanormal transform as described in Liu et al. (2009) before the structural change is learned.

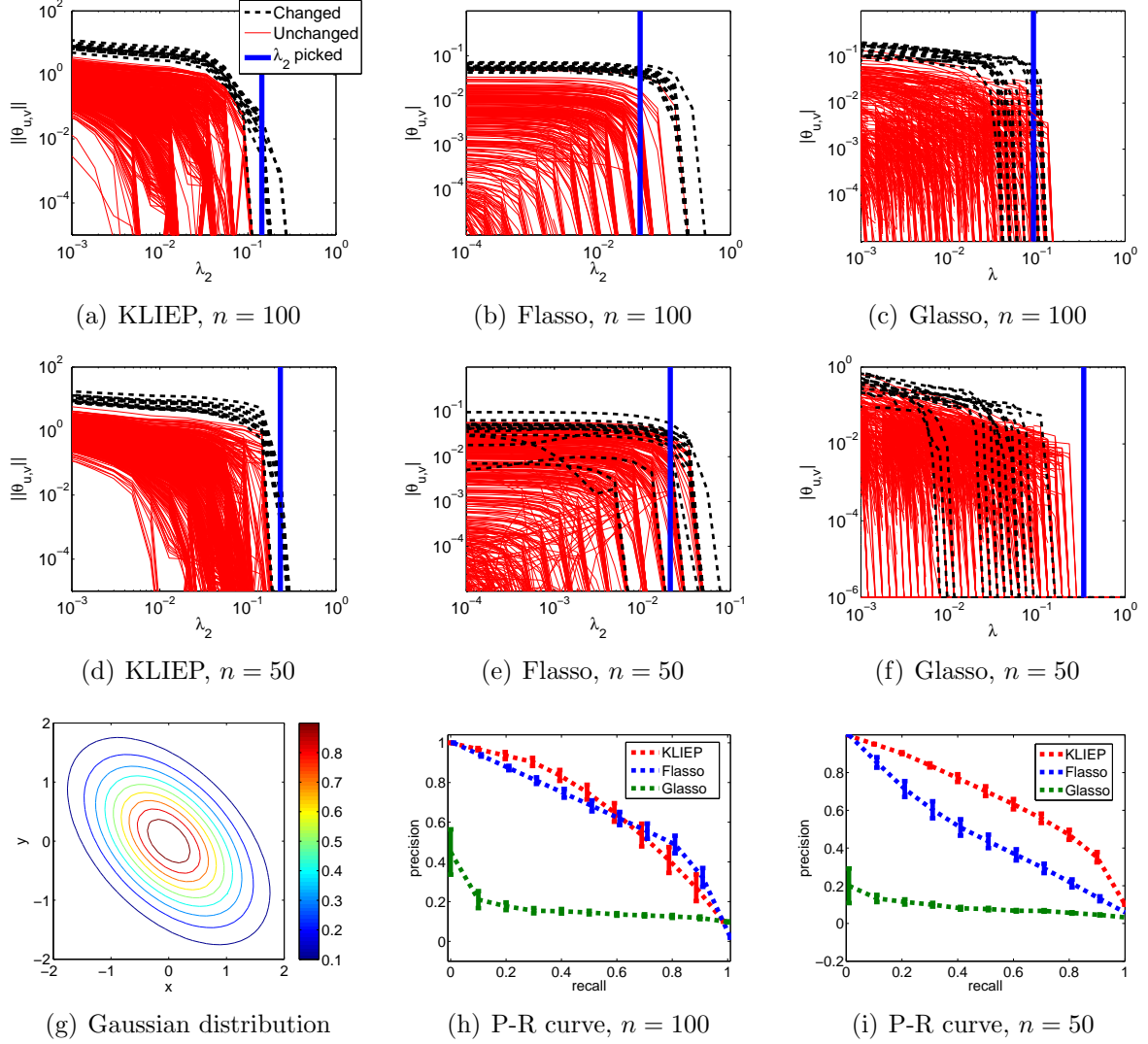


Figure 3: Experimental results on the Gaussian dataset.

The experiments are conducted on 20 randomly generated datasets with $n = 50$ and 100, respectively. The regularization paths, data generating distribution, and averaged P-R curves are plotted in Figure 4. The results show that Flasso clearly suffers from the performance degradation compared with the Gaussian case, perhaps because the number of samples is too small for the complicated nonparanormal distribution. Due to the two-step estimation scheme, the performance of Glasso is poor. In contrast, KLIEP separates changed and unchanged edges still clearly for both $n = 50$ and $n = 100$. The P-R curves also show the same tendency.

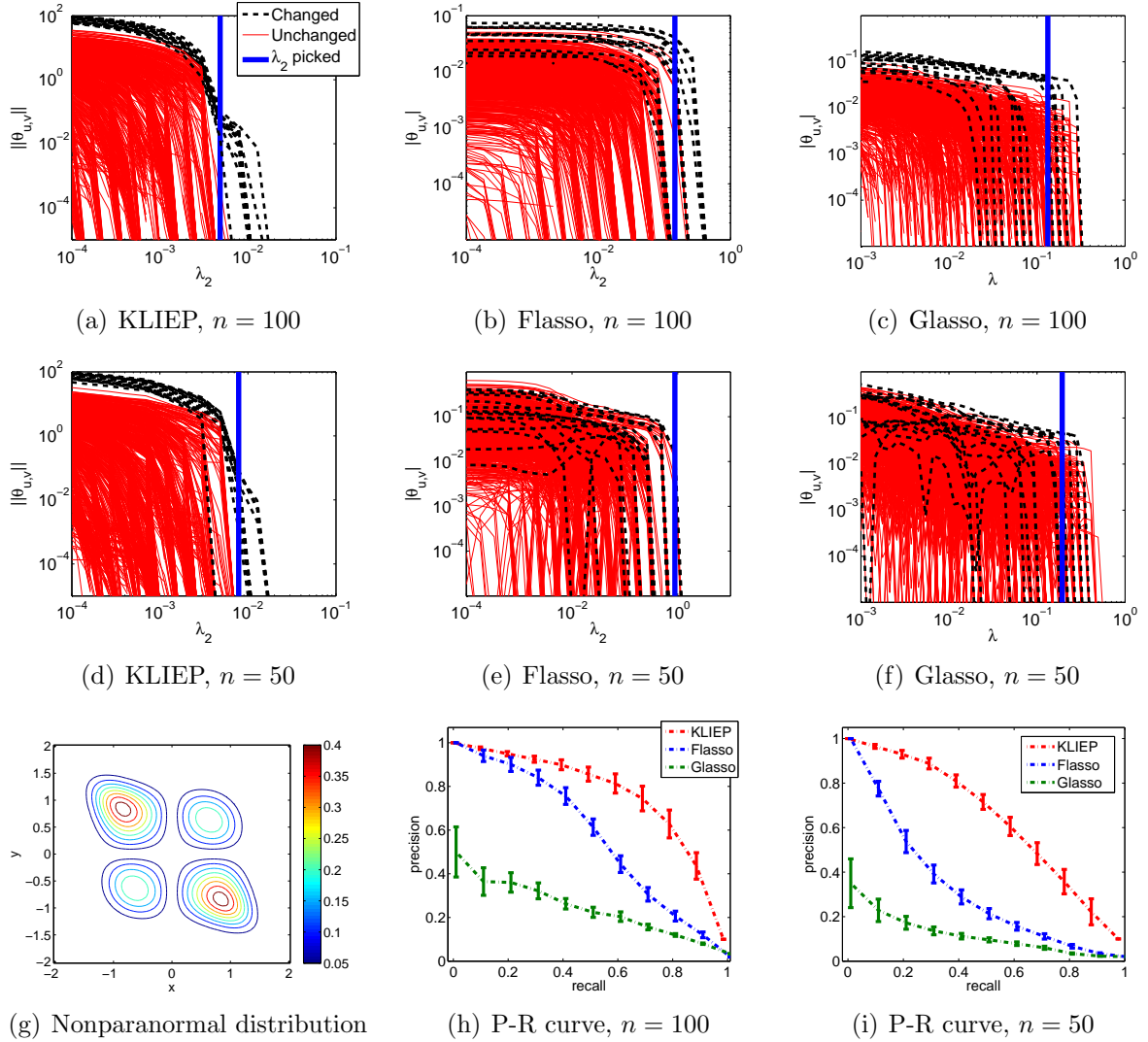


Figure 4: Experimental results on the nonparanormal dataset.

4.3 “Diamond” Distribution with No Pearson Correlation

In the experiments in Section 4.2, though samples are non-Gaussian, the *Pearson correlation* is not zero. Therefore, methods assuming Gaussianity can still capture some linear correlation between random variables. Here, we consider a more challenging case with a diamond-shaped distribution within the exponential family that has zero Pearson correlation between variables. Thus, the methods assuming Gaussianity cannot extract any information in principle from this dataset.

The probability density function of the diamond distribution is defined as follows

(Figure 5(a)):

$$p(\mathbf{x}) \propto \exp \left(- \sum_{i=1}^d 2x_i^2 - \sum_{(i,j): A_{i,j} \neq 0} 20x_i^2 x_j^2 \right), \quad (9)$$

where the adjacency matrix \mathbf{A} describes the MN structure. Note that this distribution cannot be transformed into a Gaussian distribution by any nonparanormal transformations.

We set $d = 9$ and $n_P = n_Q = 5000$. \mathbf{A}^P is randomly generated with 35% sparsity, while \mathbf{A}^Q is created by randomly removing edges in \mathbf{A}^P so that the sparsity level is dropped to 15%. Samples from the above distribution are drawn by using a *slice sampling* method (Neal, 2003). Since generating samples from high-dimensional distributions is non-trivial and time-consuming, we focus on a relatively low-dimensional case. To avoid sampling error which may mislead the experimental evaluation, we also increase the sample size, so that the erratic points generated by accident will not affect the overall population.

In this experiment, we compare the performance of KLIEP, Flasso, and Glasso with the Gaussian model, the power nonparanormal model, and the polynomial model:

$$\mathbf{f}(x_i, x_j) = (x_i^k, x_j^k, x_i x_j^{k-1}, \dots, x_i^{k-1} x_j, x_i^{k-1}, x_j^{k-1}, \dots, x_i, x_j, 1)^\top \text{ for } i \neq j.$$

The univariate polynomial transform is defined as $\mathbf{f}(x_i, x_i) = \mathbf{f}(x_i, 0)$. We test $k = 2, 3, 4$ and choose the best one in terms of HOLL. The Flasso and Glasso methods for the polynomial model are computed by importance sampling, i.e., we use the IS-Flasso and IS-Glasso methods (see Section 2.5). Since these methods are computationally very expensive, we only test $k = 4$ which we found to be a reasonable choice. We set the instrumental distribution p' as the standard normal $\mathcal{N}(\mathbf{0}, \mathbf{I})$, and use sample $\{\mathbf{x}'_i\}_{i=1}^{70000} \sim p'$ for approximating integrals. p' is purposely chosen so that it has a similar “bell” shape to the target densities but with larger variance on each dimension.

The averaged P-R curves over 20 datasets are shown in Figure 5(e). KLIEP with the polynomial model significantly outperforms all the other methods, while the IS-Glasso and especially IS-Flasso give better result than the KLIEP, Flasso, and Glasso methods with the Gaussian and nonparanormal models. This means that the polynomial basis function is indeed helpful in handling completely non-Gaussian data. However, as discussed in Section 2.2, it is difficult to use such a basis function in Glasso and Flasso because of the computational intractability of the normalization term. Although IS-Glasso can approximate integrals, the result shows that such approximation of integrals does not lead to a very good performance. In comparison, the result of the IS-Flasso method is much improved thanks to the coupled sparsity regularization, but it is still not comparable to KLIEP.

The regularization paths of KLIEP with the polynomial model illustrated in Figure 5(b) show the usefulness of the proposed method in change detection under non-Gaussianity. We also give regularization paths obtained by the IS-Flasso and IS-Glasso methods on the same dataset in Figures 5(c) and 5(d), respectively. The graphs show that both methods do not separate changed and unchanged edges well, though the IS-Flasso method works slightly better.

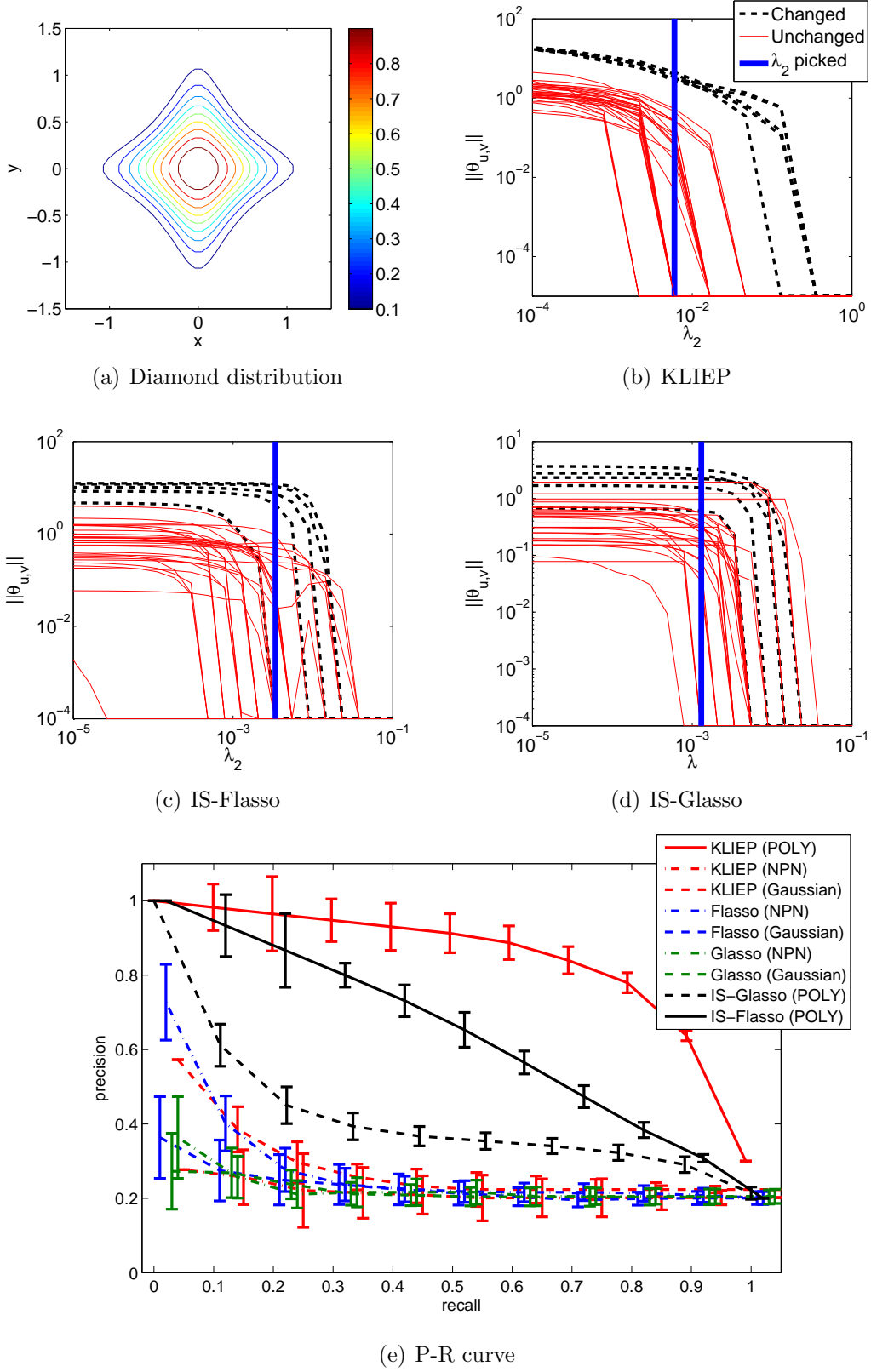


Figure 5: Experimental results on the diamond dataset. “NPN” and “POLY” denote the nonparanormal and polynomial models, respectively. Note that the precision rate of 100% recall for a random guess is approximately 20%.

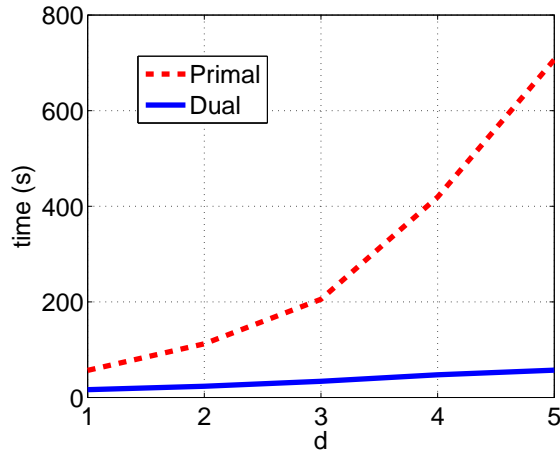


Figure 6: Comparison of computation time for solving primal and dual optimization problems.

4.4 Computation Time: Dual versus Primal Optimization Problems

Finally, we compare the computation time of the proposed KLIEP method when solving the dual optimization problem (7) and the primal optimization problem (6). Both the optimization problems are solved by using the same convex optimizer *minFunc*⁷. The datasets are generated from two Gaussian distributions constructed in the same way as Section 4.1. 150 samples are separately drawn from two distributions with dimension $d = 40, 50, 60, 70, 80$. We then perform change detection by computing the regularization paths using 20 choices of λ_2 ranging from 10^{-4} to 10^0 and fix $\lambda_1 = 0.1$. The results are plotted in Figure 6.

It can be seen from the graph that as the dimensionality increases, the computation time for solving the primal optimization problem is sharply increased, while that for solving the dual optimization problem grows only moderately: when $d = 80$, the computation time for obtaining the primal solution is almost 10 times more than that required for obtaining the dual solution. Thus, the dual formulation is computationally much more efficient than the primal formulation.

5 Applications

In this section, we report the experimental results on a synthetic gene expression dataset and a Twitter dataset.

⁷<http://www.di.ens.fr/~mschmidt/Software/minFunc.html>

5.1 Synthetic Gene Expression Dataset

A gene regulatory network encodes interactions between DNA segments. However, the way genes interact may change due to environmental or biological stimuli. In this experiment, we focus on detecting such changes. We use *SynTReN*, which is a generator of gene regulatory networks used for benchmark validation of bioinformatics algorithms (Van den Bulcke et al., 2006).

We first choose a sub-network containing 13 nodes from an existing signaling network in *Saccharomyces cerevisiae* (shown in Figure 7(a)). Three types of interactions are modeled: activation (ac), deactivation (re), and dual (du). 50 samples are generated in the first stage, after which we change the types of interactions in 6 edges, and generate 50 samples again. Four types of changes are considered: $ac \rightarrow re$, $re \rightarrow ac$, $du \rightarrow ac$, and $du \rightarrow re$.

We use KLIEP and IS-Flasso with the polynomial transform function for $k \in \{2, 3, 4\}$. The regularization parameter λ_1 in KLIEP and Flasso is tested with choices $\lambda_1 \in \{0.1, 1, 10\}$. We set the instrumental distribution p' as the standard normal $\mathcal{N}(\mathbf{0}, \mathbf{I})$, and use sample $\{\mathbf{x}'_i\}_{i=1}^{70000} \sim p'$ for approximating integrals in IS-Flasso.

The regularization paths on one example dataset for KLIEP, IS-Flasso, and the plain Flasso with the Gaussian model are plotted in Figures 7(b), 7(c), and 7(d), respectively. Averaged P-R curves over 20 simulation runs are shown in Figure 7(e). We can see clearly from the KLIEP regularization paths shown in Figure 7(b) that the magnitude of estimated parameters on the changed pairwise interactions is much higher than that of the unchanged edges. IS-Flasso also achieves rather clear separation between changed and unchanged interactions, though there are a few unchanged interactions drop to zero at the final stage. Flasso gives many false alarms by assigning non-zero values to the unchanged edges, even after some changed edges hit zeros.

Reflecting a similar pattern, the P-R curves plotted in Figure 7(e) show that the proposed KLIEP method has the best performance among all three methods. We can also see that the IS-Flasso method achieves significant improvement over the plain Flasso method with the Gaussian model. The improvement from Flasso to IS-Flasso shows that the use of the polynomial basis is useful on this dataset, and the improvement from IS-Flasso to KLIEP shows that the direct estimation can further boost the performance.

5.2 Twitter Story Telling

Finally, we use KLIEP with the polynomial transform function for $k \in \{2, 3, 4\}$ and Flasso as event detectors from Twitter. More specifically, we choose the *Deepwater Horizon oil spill*⁸ as the target event, and we hope that our method can recover some story lines from Twitter as the news events develop. Counting the frequencies of 10 keywords (BP, oil, spill, Mexico, gulf, coast, Hayward, Halliburton, Transocean, and Obama), we obtain a dataset by sampling 4 times per day from February 1st, 2010 to October 15th, 2010, resulting in 1061 data samples.

⁸http://en.wikipedia.org/wiki/Deepwater_Horizon_oil_spill

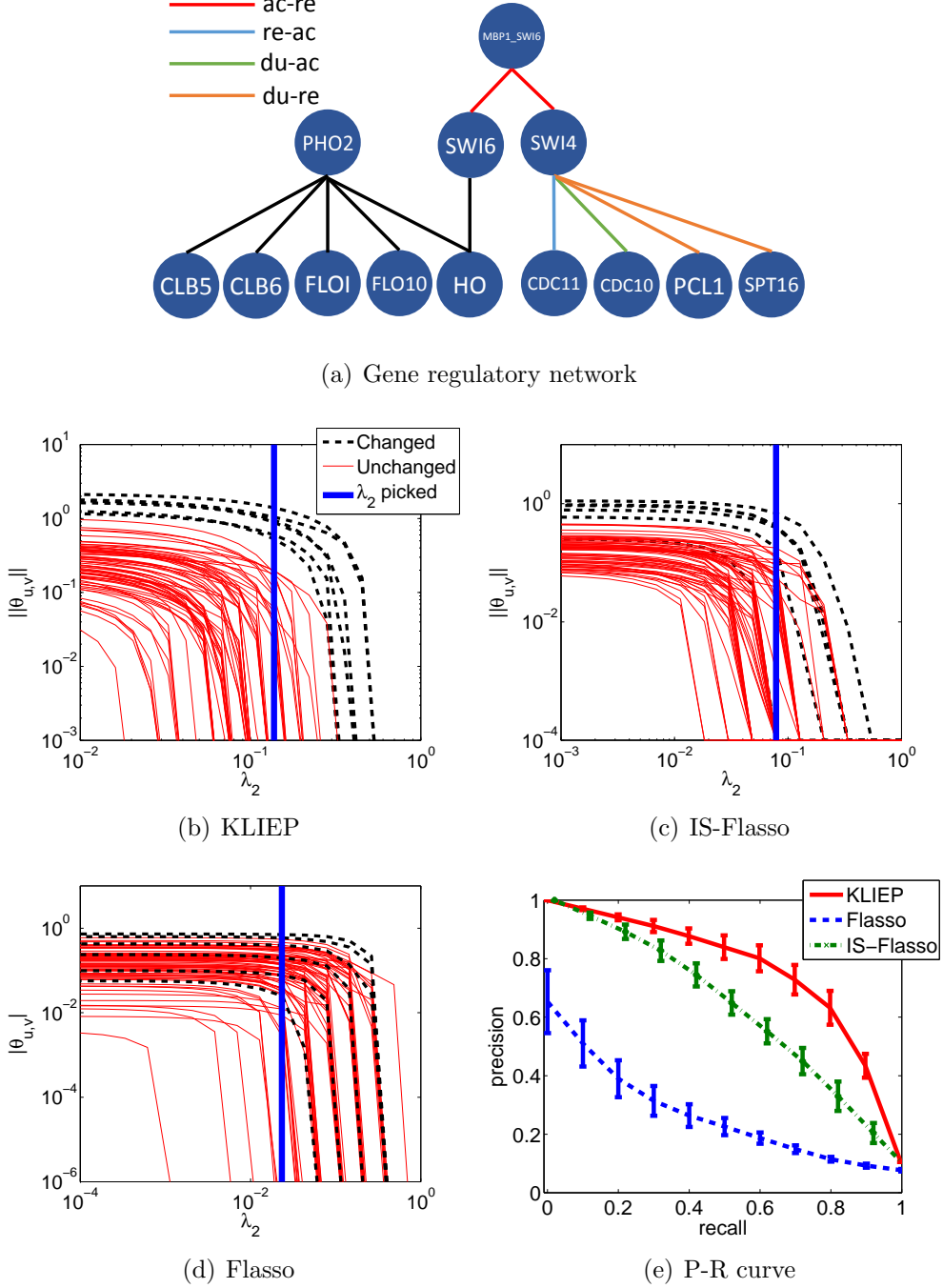


Figure 7: Experiments on synthetic gene expression datasets.

We segment the data into two parts: the first 300 samples collected before the day of oil spill (April 20th, 2010) are regarded as conforming to a 10-dimensional joint distribution Q , while the second set of samples that are in an arbitrary 50-day window after the oil spill accident happened is regarded as following distribution P . Thus, the MN of Q encodes the original conditional independence of frequencies between 10 keywords, while the underlying MN of P has changed since an event occurred. We expect that unveiling changes in MNs between P and Q can recover the drift of popular topic trends on Twitter in terms of the dependency among keywords.

The detected change graphs (i.e., the graphs with only detected changing edges) on 10 keywords are illustrated in Figure 8. The edges are selected at a certain value of λ_2 indicated by the maximal *cross-validated log-likelihood* (CVLL). Since the edge set that is picked by CVLL may not be sparse in general, we sparsify the graph based on the permutation test as follows: we randomly shuffle the samples between P and Q and repeatedly run change detection algorithms for 100 times; then we observe detected edges by CVLL. Finally, we select the edges that are detected using the original non-shuffled dataset and remove those that were detected in the shuffled datasets for more than 5 times (i.e., the significance level 5%). For KLIEP, k is also tuned by using CVLL. In Figure 8, we plot detected change graphs which are generated using samples of P starting from April 17th, July 6th, and July 26th, respectively.

The initial explosion happened on April 20th, 2010. Both methods discover dependency changes between keywords. Generally speaking, KLIEP captures more conditional independence changes between keywords than the Flasso method, especially when comparing Figure 8(c) and Figure 8(f). At the first two stages (Figures 8(a), 8(b), 8(d) and 8(e)), the keyword “Obama” is very well connected with other keywords in the results given by both methods. Indeed, at the early development of this event, he lies in the center of the news stories, and his media exposure peaks after his visit to the Louisiana coast (May 2nd, May 28nd, and June 5th) and his meeting with BP CEO Tony Hayward on June 16th. Notably, both methods highlight the “gulf-obama-coast” triangle in Figures 8(a) and 8(d) and the “bp-obama-hayward” chain in Figures 8(b) and 8(e).

However, there are some important differences worth mentioning. First, the Flasso method misses the “transocean-hayward-obama” triangle in Figures 8(d) and 8(e). Transocean is the contracted operator in the Deepwater Horizon platform, where the initial explosion happened. On Figure 8(c), the chain “bp-spill-oil” may indicate that the phrase “bp spill” or “oil spill” has been publicly recognized by the Twitter community since then, while the “hayward-bp-mexico” triangle, although relatively weak, may link to the event that Hayward stepped down from the CEO position on July 27th.

It is also noted that Flasso cannot find any changed edges in Figure 8(f), perhaps due to the Gaussian restriction.

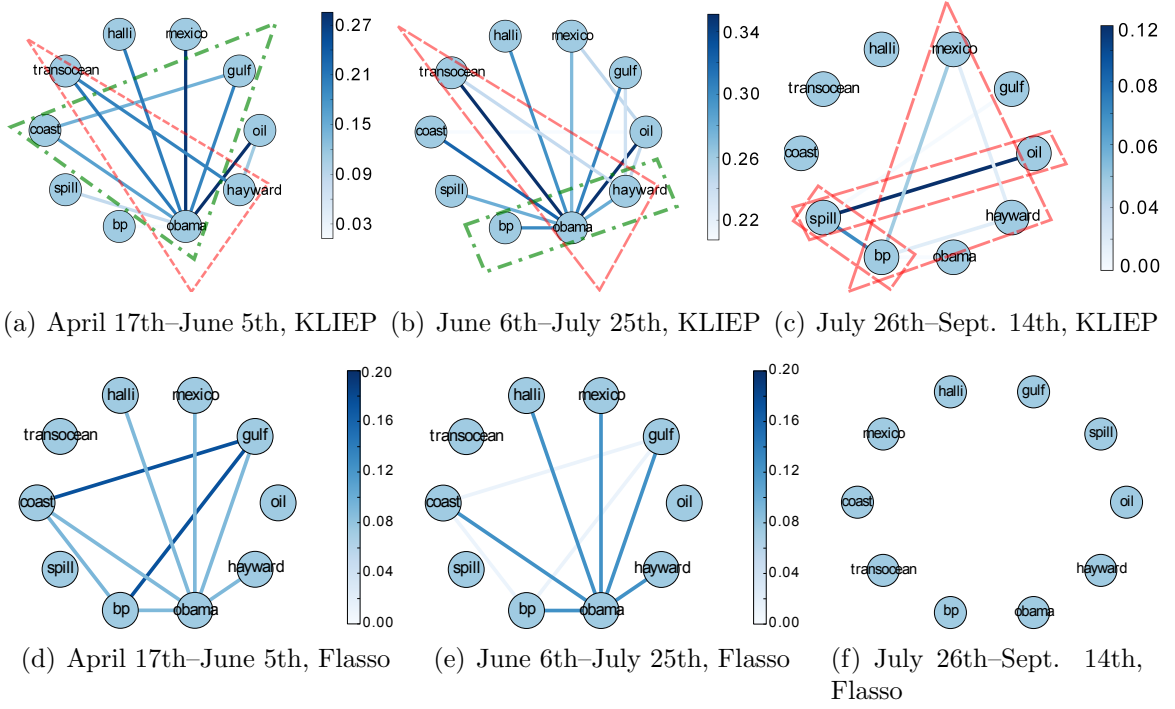


Figure 8: Change graphs captured by the proposed KLIEP method (top) and the Flasso method (bottom). The date range beneath each figure indicates when P was sampled, while Q is fixed to dates from February 1st to April 20th. Notable structures shared by the graph of both methods are surrounded by the dash-dotted lines. Unique structures that only appear in the graph of the proposed KLIEP method are surrounded by the dashed lines.

6 Discussion, Conclusion, and Future Works

In this paper, we proposed a *direct* approach to learning sparse changes in MNs by density ratio estimation. Rather than fitting two MNs separately to data and comparing them to detect a change, we estimated the ratio of the probability densities of two MNs where changes can be naturally encoded as sparsity patterns in estimated parameters. This direct modeling allows us to halve the number of parameters and approximate the normalization term in the density ratio model by a sample average without sampling. We also showed that the number of parameters to be optimized can be further reduced with the dual formulation, which is highly useful when the dimensionality is high. Through experiments on artificial and real-world datasets, we demonstrated the usefulness of the proposed method over state-of-the-art methods including nonparanormal-based methods and sampling-based methods.

Our important future work is to theoretically elucidate the advantage of the proposed method, beyond the Vapnik’s principle of solving the target problem directly. The relation to *score matching* (Hyvärinen, 2005), which avoids computing the normalization term in

density estimation, is also an interesting issue to be further investigated. Considering higher-order MN models such as the *hierarchical log-linear model* (Schmidt and Murphy, 2010) is a promising direction for extension.

In the context of change detection, we are mainly interested in the situation where p and q are close to each other (if p and q are completely different, it is straightforward to detect changes). When p and q are similar, density ratio estimation for $p(\mathbf{x})/q(\mathbf{x})$ or $q(\mathbf{x})/p(\mathbf{x})$ perform similarly. However, given the asymmetry of density ratios, the solutions for $p(\mathbf{x})/q(\mathbf{x})$ or $q(\mathbf{x})/p(\mathbf{x})$ are generally different. The choice of the numerator and denominator in the ratio is left for future investigation.

Detecting changes in MNs is the main target of this paper. On the other hand, estimating the difference/divergence between two probability distributions has been studied under a more general context in the statistics and machine learning communities (Amari and Nagaoka, 2000; Eguchi and Copas, 2006; Wang et al., 2009; Sugiyama et al., 2012b, 2013a). In fact, the estimation of the *Kullback-Leibler divergence* (Kullback and Leibler, 1951) is related to the KLIEP-type density ratio estimation method (Nguyen et al., 2010), and the estimation of the *Pearson divergence* (Pearson, 1900) is related to the squared-loss density ratio estimation method (Kanamori et al., 2009). However, the density ratio based divergences tend to be sensitive to outliers. To overcome this problem, a divergence measure based on relative density ratios was introduced, and its direct estimation method was developed (Yamada et al., 2013). L^2 -distance is another popular difference measure between probability density functions. L^2 -distance is symmetric, unlike the Kullback-Leibler divergence and the Pearson divergence, and its direct estimation method has been investigated recently (Sugiyama et al., 2013b; Kim and Scott, 2010).

Change detection in time-series is a related topic. A straightforward approach is to evaluate the difference (dissimilarity) between two consecutive segments of time-series signals. Various methods have been developed to identify the difference by fitting two models to two segments of time-series separately, e.g., the singular spectrum transform (Moskvina and Zhigljavsky, 2003; Ide and Tsuda, 2007), subspace identification (Kawahara et al., 2007), and the method based on the one-class support vector machine (Desobry et al., 2005). In the same way as the current paper, directly modeling of the change has also been explored for change detection in time-series (Kawahara and Sugiyama, 2012; Liu et al., 2013; Sugiyama et al., 2013b).

Acknowledgements

SL is supported by the JST PRESTO program and the JSPS fellowship. JQ is supported by the JST PRESTO program. MUG is supported by the Finnish Centre-of-Excellence in Computational Inference Research COIN (251170). TS is partially supported by MEXT Kakenhi 25730013, and the Aihara Project, the FIRST program from JSPS, initiated by CSTP. MS is supported by the JST CREST program and AOARD.

Appendix: Derivation of the Dual Optimization Problem

First, we rewrite the optimization problem (6) as

$$\begin{aligned} \min_{\boldsymbol{\theta}, \mathbf{w}} \left[\log \left(\sum_{i=1}^{n_Q} \exp(w_i) \right) - \boldsymbol{\theta}^\top \mathbf{g} + \frac{\lambda_1}{2} \boldsymbol{\theta}^\top \boldsymbol{\theta} + \lambda_2 \sum_{u \geq v} \|\boldsymbol{\theta}_{u,v}\| - C \right] \\ \text{subject to } \mathbf{w} = \mathbf{H}^\top \boldsymbol{\theta}, \end{aligned} \quad (10)$$

where

$$\begin{aligned} \mathbf{w} &= (w_1, \dots, w_{n_Q})^\top, \\ \mathbf{H} &= (\mathbf{H}_{1,1}^\top, \dots, \mathbf{H}_{d,1}^\top, \mathbf{H}_{2,2}^\top, \dots, \mathbf{H}_{d,2}^\top, \dots, \mathbf{H}_{d,d}^\top)^\top, \\ \mathbf{H}_{u,v} &= [\mathbf{f}(x_1^{(u)Q}, x_1^{(v)Q}), \dots, \mathbf{f}(x_{n_Q}^{(u)Q}, x_{n_Q}^{(v)Q})], \\ \mathbf{g} &= (\mathbf{g}_{1,1}^\top, \dots, \mathbf{g}_{d,1}^\top, \mathbf{g}_{2,2}^\top, \dots, \mathbf{g}_{d,2}^\top, \dots, \mathbf{g}_{d,d}^\top)^\top, \\ \mathbf{g}_{u,v} &= \frac{1}{n_P} \sum_{i=1}^{n_P} \mathbf{f}(x_i^{(u)P}, x_i^{(v)P}), \\ C &= \log n_Q. \end{aligned}$$

With Lagrange multipliers $\boldsymbol{\alpha} = (\alpha_1, \dots, \alpha_{n_Q})^\top$, the Lagrangian of (10) is given as

$$\begin{aligned} \mathcal{L}(\boldsymbol{\alpha}) &= \min_{\mathbf{w}, \boldsymbol{\theta}} \left[\log \sum_{i=1}^{n_Q} \exp(w_i) - \boldsymbol{\theta}^\top \mathbf{g} + \frac{\lambda_1}{2} \boldsymbol{\theta}^\top \boldsymbol{\theta} + \lambda_2 \sum_{u \geq v} \|\boldsymbol{\theta}_{u,v}\| - (\mathbf{w} - \mathbf{H}^\top \boldsymbol{\theta})^\top \boldsymbol{\alpha} \right] - C \\ &= \min_{\mathbf{w}} \left[\log \sum_{i=1}^{n_Q} \exp(w_i) - \mathbf{w}^\top \boldsymbol{\alpha} \right] \\ &\quad + \min_{\boldsymbol{\theta}} \left[\boldsymbol{\theta}^\top (\mathbf{H} \boldsymbol{\alpha} - \mathbf{g}) + \frac{\lambda_1}{2} \boldsymbol{\theta}^\top \boldsymbol{\theta} + \lambda_2 \sum_{u \geq v} \|\boldsymbol{\theta}_{u,v}\| \right] - C \\ &= \min_{\mathbf{w}} \psi_1(\mathbf{w}) + \min_{\boldsymbol{\theta}} \psi_2(\boldsymbol{\theta}) - C. \end{aligned} \quad (11)$$

A few lines of algebra can show that $\psi_1(\mathbf{w})$ reaches the minimum $-\sum_{i=1}^{n_Q} \alpha_i \log \alpha_i$ at

$$\alpha_i = \frac{\exp(w_i)}{\sum_{i=1}^{n_Q} \exp(w_i)}, \quad i = 1, \dots, n_Q.$$

Note that extra constraints are implied from the above equation:

$$\alpha_1, \dots, \alpha_{n_Q} \geq 0 \text{ and } \sum_{i=1}^{n_Q} \alpha_i = 1.$$

Since $\psi_2(\boldsymbol{\theta})$ is not differentiable at $\boldsymbol{\theta}_{u,v} = \mathbf{0}$, we can only obtain its sub-gradient:

$$\nabla_{\boldsymbol{\theta}_{u,v}} \psi_2(\boldsymbol{\theta}) = -\boldsymbol{\xi}_{u,v} + \lambda_1 \boldsymbol{\theta} + \lambda_2 \nabla_{\boldsymbol{\theta}_{u,v}} \|\boldsymbol{\theta}_{u,v}\|,$$

where

$$\begin{aligned} \boldsymbol{\xi}_{u,v} &= \mathbf{g}_{u,v} - \mathbf{H}_{u,v} \boldsymbol{\alpha}, \\ \nabla_{\boldsymbol{\theta}_{u,v}} \|\boldsymbol{\theta}_{u,v}\| &= \begin{cases} \frac{\boldsymbol{\theta}_{u,v}}{\|\boldsymbol{\theta}_{u,v}\|} & \text{if } \boldsymbol{\theta}_{u,v} \neq \mathbf{0}, \\ \{\mathbf{y} \mid \|\mathbf{y}\| \leq 1\} & \text{if } \boldsymbol{\theta}_{u,v} = \mathbf{0}. \end{cases} \end{aligned}$$

By setting $\nabla_{\boldsymbol{\theta}_t} \psi_2(\boldsymbol{\theta}) = \mathbf{0}$, we can obtain the solution to this minimization problem by Eq.(8).

Substituting the solutions of the above two minimization problems with respect to $\boldsymbol{\theta}$ and \mathbf{w} into (11), we obtain the dual optimization problem (7).

References

- S. Amari and H. Nagaoka. *Methods of Information Geometry*. Oxford University Press, Providence, RI, USA, 2000.
- O. Banerjee, L. El Ghaoui, and A. d’Aspremont. Model selection through sparse maximum likelihood estimation for multivariate Gaussian or binary data. *Journal of Machine Learning Research*, 9:485–516, March 2008.
- C. M. Bishop. *Pattern Recognition and Machine Learning*. Springer, New York, NY, USA, 2006.
- S. Boyd and L. Vandenberghe. *Convex Optimization*. Cambridge University Press, Cambridge, UK, 2004.
- P. Danaher, P. Wang, and D. M. Witten. The joint graphical lasso for inverse covariance estimation across multiple classes. *Journal of the Royal Statistical Society: Series B (Statistical Methodology)*, 2013.
- F. Desobry, M. Davy, and C. Doncarli. An online kernel change detection algorithm. *IEEE Transactions on Signal Processing*, 53(8):2961–2974, 2005.
- S. Eguchi and J. Copas. Interpreting Kullback-Leibler divergence with the Neyman-Pearson lemma. *Journal of Multivariate Analysis*, 97(9):2034–2040, 2006.
- J. Friedman, T. Hastie, and R. Tibshirani. Sparse inverse covariance estimation with the graphical lasso. *Biostatistics*, 9(3):432–441, 2008.
- A. Gelman. Method of moments using Monte Carlo simulation. *Journal of Computational and Graphical Statistics*, 4(1):36–54, 1995.

- M. U. Gutmann and A. Hyvärinen. Noise-contrastive estimation of unnormalized statistical models, with applications to natural image statistics. *Journal of Machine Learning Research*, 13:307–361, 2012.
- T. Hastie, R. Tibshirani, and J. Friedman. *The Elements of Statistical Learning: Data Mining, Inference, and Prediction*. Springer, New York, NY, USA, 2001.
- G. E. Hinton. Training products of experts by minimizing contrastive divergence. *Neural computation*, 14(8):1771–1800, 2002.
- A. Hyvärinen. Estimation of non-normalized statistical models by score matching. *Journal of Machine Learning Research*, 6:695–709, 2005.
- T. Ide and K. Tsuda. Change-point detection using Krylov subspace learning. In *Proceedings of the SIAM International Conference on Data Mining*, pages 515–520, 2007.
- T. Kanamori, S. Hido, and M. Sugiyama. A least-squares approach to direct importance estimation. *Journal of Machine Learning Research*, 10:1391–1445, 2009.
- T. Kanamori, T. Suzuki, and M. Sugiyama. Theoretical analysis of density ratio estimation. *IEICE Transactions on Fundamentals of Electronics, Communications and Computer Sciences*, E93-A(4):787–798, 2010.
- Y. Kawahara and M. Sugiyama. Sequential change-point detection based on direct density-ratio estimation. *Statistical Analysis and Data Mining*, 5(2):114–127, 2012.
- Y. Kawahara, T. Yairi, and K. Machida. Change-point detection in time-series data based on subspace identification. In *Proceedings of the 7th IEEE International Conference on Data Mining*, pages 559–564, 2007.
- J. Kim and C. Scott. L_2 kernel classification. *IEEE Transactions on Pattern Analysis and Machine Intelligence*, 32(10):1822–1831, 2010.
- D. Koller and N. Friedman. *Probabilistic Graphical Models: Principles and Techniques*. MIT Press, 2009.
- S. Kullback and R. A. Leibler. On information and sufficiency. *The Annals of Mathematical Statistics*, 22:79–86, 1951.
- S.-I. Lee, V. Ganapathi, and D. Koller. Efficient structure learning of Markov networks using l_1 -regularization. In B. Schölkopf, J. Platt, and T. Hoffman, editors, *Advances in Neural Information Processing Systems 19*, pages 817–824, Cambridge, MA, 2007. MIT Press.
- H. Liu, J. Lafferty, and L. Wasserman. The nonparanormal: Semiparametric estimation of high dimensional undirected graphs. *Journal of Machine Learning Research*, 10:2295–2328, 2009.

- 492 H. Liu, F. Han, M. Yuan, J. Lafferty, and L. Wasserman. The nonparanormal skeptic. In
493 *Proceedings of the 29th International Conference on Machine Learning (ICML2012)*,
494 2012.
- 495 S. Liu, M. Yamada, N. Collier, and M. Sugiyama. Change-point detection in time-series
496 data by relative density-ratio estimation. *Neural Networks*, 43:72–83, 2013.
- 497 N. Meinshausen and P. Bühlmann. High-dimensional graphs and variable selection with
498 the lasso. *The Annals of Statistics*, 34(3):1436–1462, 2006.
- 499 V. Moskvina and A. Zhigljavsky. Change-point detection algorithm based on the singular-
500 spectrum analysis. *Communications in Statistics: Simulation and Computation*, 32:
501 319–352, 2003.
- 502 R. M Neal. Slice sampling. *The Annals of Statistics*, 31(3):705–741, 2003.
- 503 X. Nguyen, M. J. Wainwright, and M. I. Jordan. Estimating divergence functionals and
504 the likelihood ratio by convex risk minimization. *IEEE Transactions on Information*
505 *Theory*, 56(11):5847–5861, 2010.
- 506 K. Pearson. On the criterion that a given system of deviations from the probable in the
507 case of a correlated system of variables is such that it can be reasonably supposed to
508 have arisen from random sampling. *Philosophical Magazine*, 50:157–175, 1900.
- 509 P. Ravikumar, M. J. Wainwright, and J. D. Lafferty. High-dimensional Ising model selec-
510 tion using ℓ_1 -regularized logistic regression. *The Annals of Statistics*, 38(3):1287–1319,
511 2010.
- 512 C. P. Robert and G. Casella. *Monte Carlo Statistical Methods*. Springer-Verlag, Secaucus,
513 NJ, USA, 2005.
- 514 M. W. Schmidt and K. P. Murphy. Convex structure learning in log-linear models: Beyond
515 pairwise potentials. *Journal of Machine Learning Research - Proceedings Track*, 9:709–
516 716, 2010.
- 517 M. Sugiyama, T. Suzuki, S. Nakajima, H. Kashima, P. von Bünau, and M. Kawanabe.
518 Direct importance estimation for covariate shift adaptation. *Annals of the Institute of*
519 *Statistical Mathematics*, 60(4):699–746, 2008.
- 520 M. Sugiyama, T. Suzuki, and T. Kanamori. *Density Ratio Estimation in Machine Learn-*
521 *ing*. Cambridge University Press, Cambridge, UK, 2012a.
- 522 M. Sugiyama, T. Suzuki, and T. Kanamori. Density-ratio matching under the Bregman
523 divergence: a unified framework of density-ratio estimation. *Annals of the Institute of*
524 *Statistical Mathematics*, 64(5):1009–1044, 2012b.

- 525 M. Sugiyama, S. Liu, M. C. du Plessis, M. Yamanaka, M. Yamada, T. Suzuki, and
526 T. Kanamori. Direct divergence approximation between probability distributions and
527 its applications in machine learning. *Journal of Computing Science and Engineering*, 7
528 (2):99–111, 2013a.
- 529 M. Sugiyama, T. Suzuki, T. Kanamori, M. C. du Plessis, S. Liu, and I. Takeuchi. Density-
530 difference estimation. *Neural Computation*, 25(10):2734–2775, 2013b.
- 531 R. Tibshirani, M. Saunders, S. Rosset, J. Zhu, and K. Knight. Sparsity and smooth-
532 ness via the fused lasso. *Journal of the Royal Statistical Society: Series B (Statistical
533 Methodology)*, 67(1):91–108, 2005.
- 534 Y. Tsuboi, H. Kashima, S. Hido, S. Bickel, and M. Sugiyama. Direct density ratio es-
535 timation for large-scale covariate shift adaptation. *Journal of Information Processing*,
536 17:138–155, 2009.
- 537 T. Van den Bulcke, K. Van Leemput, B. Naudts, P. van Remortel, H. Ma, A. Verschoren,
538 B. De Moor, and K. Marchal. SynTReN: A generator of synthetic gene expression data
539 for design and analysis of structure learning algorithms. *BMC Bioinformatics*, 7(1):43,
540 2006.
- 541 V. N. Vapnik. *Statistical Learning Theory*. Wiley, New York, NY, USA, 1998.
- 542 M. J. Wainwright and M. I. Jordan. Graphical models, exponential families, and varia-
543 tional inference. *Foundations and Trends® in Machine Learning*, 1(1-2):1–305, 2008.
- 544 Q. Wang, S. R. Kulkarni, and S. Verdú. Divergence estimation for multidimensional
545 densities via k-nearest-neighbor distances. *IEEE Transactions on Information Theory*,
546 55(5):2392–2405, 2009.
- 547 L. Wasserman. *All of Statistics: A Concise Course in Statistical Inference*. Springer
548 Publishing Company, Incorporated, 2010.
- 549 M. Yamada, T. Suzuki, T. Kanamori, H. Hachiya, and M. Sugiyama. Relative density-
550 ratio estimation for robust distribution comparison. *Neural Computation*, 25(5):1324–
551 1370, 2013.
- 552 B. Zhang and Y.J. Wang. Learning structural changes of Gaussian graphical models in
553 controlled experiments. In *Proceedings of the Twenty-Sixth Conference on Uncertainty
554 in Artificial Intelligence (UAI2010)*, pages 701–708, 2010.
- 555 H. Zou and T. Hastie. Regularization and variable selection via the elastic net. *Journal
556 of the Royal Statistical Society, Series B*, 67(2):301–320, 2005.